

Bimodal electroencephalography-functional magnetic resonance imaging dataset for inner-speech recognition

Foteini Simistira Liwicki^{1,*}, Vibha Gupta¹, Rajkumar Saini¹, Kanjar De¹, Nosheen Abid¹, Sumit Rakesh¹, Scott Wellington², Holly Wilson², Marcus Liwicki¹, and Johan Eriksson³

¹Luleå University of Technology, Department of Computer Science, Electrical and Space Engineering, Embedded Intelligent Systems LAB, Sweden

²University of Bath, Department of Computer Science, United Kingdom

³Umeå University, Department of Integrative Medical Biology (IMB) and Umeå Center for Functional Brain Imaging (UFBI), Sweden

ABSTRACT

The recognition of inner speech, which could give a ‘voice’ to patients that have no ability to speak or move, is a challenge for brain-computer interfaces (BCIs). A shortcoming of the available datasets is that they do not combine modalities to increase the performance of inner speech recognition. Multimodal datasets of brain data enable the fusion of neuroimaging modalities with complimentary properties, such as the high spatial resolution of functional magnetic resonance imaging (fMRI) and the temporal resolution of electroencephalography (EEG), and therefore are promising for decoding inner speech. This paper presents the first publicly available bimodal dataset containing EEG and fMRI data acquired nonsimultaneously during inner-speech production. Data were obtained from four healthy, right-handed participants during an inner-speech task with words in either a social or numerical category. Each of the 8-word stimuli were assessed with 40 trials, resulting in 320 trials in each modality for each participant. The aim of this work is to provide a publicly available bimodal dataset on inner speech, contributing towards speech prostheses.

Background & Summary

Although research in the field of brain-computer interfaces (BCIs) began in the 1960s, it has accelerated in recent years due to advances in machine learning, imaging, and other data collection modalities.^{1,2} A core aim of BCI research is to assist people who have lost the ability to move, speak or communicate with their environment. Inner speech can be described as the inner voice inside our heads; this phenomenon is used when thinking in a language without any accompanying muscle movement or speech articulation³⁻⁶. Decoding inner speech from brain activity is a burgeoning research area and has applications for BCI paradigms such as speech prostheses^{7,8}, in clinical contexts—for example, informing models of psychiatric disorders in which inner speech is disturbed (e.g., schizophrenia^{9,10})—and in neuroscience, by deepening our understanding of the spatiotemporal neural dynamics of inner speech¹¹.

Preliminary results have revealed that the most important parts of the brain for inner speech are the frontal gyri, including Broca’s area, the supplementary motor area and the precentral gyrus^{12,13}. Furthermore, core representations of the language system (phonology, lexicon, and syntax) have a clearly distinguishable spatial distribution in the neocortex¹⁴⁻¹⁶. This distribution of brain regions is remarkably similar across languages and across individuals¹⁷, regardless of why these language representations are accessed (i.e., for production or comprehension) or how they are accessed (i.e., visually (by reading) or auditorily (by listening)).

BCI technologies use brain data acquired by invasive (e.g., electrocorticography (ECoG)¹⁸) or noninvasive modalities (e.g., electroencephalography (EEG)¹⁹, functional magnetic resonance imaging (fMRI)²⁰, functional near-infrared spectroscopy (fNIRS)^{21,22} and magnetoencephalography (MEG)^{23,24}) to establish an interface between humans and machines; in particular EEG data are the most commonly used in BCIs; and fMRI is a typical complimentary modality due to high spatial resolution. BCI paradigms include motor imagery^{25,26} and external stimulation paradigms, such as the visual P300²⁷. In motor imagery paradigms, patients imagine their movement without overtly performing the action; in the visual P300 paradigm, patients typically use the direction of their eye gaze to spell out words by selecting among flashing stimuli, again without additional overt movement, which requires substantial participant concentration²⁸. Thus, in recent years, the research focus for BCIs used to enable Augmentative and Alternative Communications (AACs) has turned to inner speech.

37 Research on inner speech decoding has investigated the use of all invasive ECoG^{29,30} and noninvasive methods^{31–35}.
38 Various datasets have been acquired. Selected studies presenting EEG and fMRI are as follows: KARA ONE³⁶ is a dataset
39 of inner and outer speech recordings that combines a 62-channel EEG with facial and audio data. The dataset includes 12
40 participants, and the lexicon contains 7 phonemes and 4 phonetically-similar words for binary phonological classification.
41 Coretto *et al.*³⁷ provided a dataset containing a 6-channel EEG recordings of inner and outer speech recordings of 5 vowels
42 and 6 words. Nguyen *et al.*³⁸ generated a dataset that contains a 64-channel EEG recordings of inner speech from 15 subjects,
43 with a lexicon of 3 vowels and 5 words (note that the work also introduces new algorithms, but this is secondary for our study).
44 Ferreira *et al.*³⁹ provided a fMRI dataset of inner speech recordings from 20 native Portuguese speakers that consisted of
45 cardinal vowels, monosyllabic and disyllabic words, and sentences. Recently, Nieto *et al.*⁴⁰ published an open-source unimodal
46 EEG dataset of inner-speech BCI commands in Spanish.

47 The main limitation of such unimodal datasets is a much lower bound for possible recognition performance, as either
48 temporal or spatial aspects of the data are not included. Unimodal datasets based on either EEG or fMRI can have drawbacks
49 with regard to their temporal and spatial resolutions; specifically EEG datasets suffer from low spatial resolution but have a
50 high temporal resolution, whereas fMRI datasets have a high spatial resolution that provides a deeper look into the subcortical
51 structures of the brain but is limited by low temporal resolution. The relative strengths and weaknesses of these two neuroimaging
52 modalities make their combination complimentary for brain analyses.

53 As for the combination of different modalities, recent studies on tasks different to inner-speech decoding have shown a
54 possible improvement of the neural decoding performance^{41–44}. Perronnet *et al.*⁴¹ found that haemodynamic and electrophysio-
55 logical activity during motor imagery tasks was higher when combining EEG and fMRI data compared to when EEG or fMRI
56 data were used alone. Lioi *et al.*'s⁴³ neurofeedback-based dataset of bimodal motor imagery was acquired with simultaneous
57 EEG-fMRI recordings; the data were recorded from 30 subjects performing kinaesthetic motor-imagery tasks with the right
58 hand to bring a ball to a target. In this work, the simultaneous bimodal EEG and fMRI dataset shows the potential of improving
59 the quality of neurofeedback during a motor-imagery task compared to when using only one modality. Berezutskaya *et al.*⁴⁴
60 created a publicly-available multimodal nonsimultaneous dataset consisting of ECoG and fMRI data involving naturalistic
61 simulation with a short audio-visual film; the dataset contains ECoG data from 51 subjects (5-55 years of age) and fMRI data
62 from 30 participants (7-47 years of age) on the same task, enabling between-modality and subject-similarity analyses. This
63 bimodal dataset shows the potential of combining different modalities to improve the study of neural mechanisms during
64 language understanding and perception. The major outcomes of these studies were an improvement of the analysis when data
65 from different modalities were combined. Making use of modality combination, hence, would be promising for inner-speech
66 decoding as well.

67 The closest related work to this study is Cooney *et al.*⁴², which generated a bimodal dataset of EEG (64-channel) and
68 fNIRS (8-channel) data by acquiring simultaneous recordings from 19 subjects during outer and inner speech. However, the
69 improvement in the performance in the task of inner-speech decoding was not as significant. Specifically, fNIRS showed a low
70 decoding performance, and the use of the fNIRS modality was proven not significant for the bimodal decoding. Therefore, the
71 choice of this work is to focus on EEG without fNIRS.

72 In terms of simultaneous vs nonsimultaneous recordings, we decided to choose nonsimultaneous recordings. Following
73 the assessment procedure proposed by Scrivener⁴⁵, we weighed in the following reasons: the analysis does not require
74 simultaneously recorded data and it is not acceptable that the EEG data contain more artifacts when recorded with fMRI.
75 Furthermore, nonsimultaneous recordings enable optimization of the task for each modality, such as fast paradigms with EEG
76 and slow paradigms with fMRI, which has a slow BOLD response, therefore optimal for the bimodal acquisition of EEG and
77 fMRI when comes to the inner-speech task.

78 The aim of this study was to collect separately-recorded EEG and fMRI recordings from healthy participants, performing
79 an inner-speech task that followed the same experimental protocol for both modalities. This study showed that combining
80 separately-recorded EEG and fMRI data can facilitate the decoding of inner speech, as this approach combines both high
81 temporal and spatial resolution. To the best of our knowledge, this study represents the first publicly available dataset with
82 bimodal nonsimultaneous EEG and fMRI recordings of inner speech. This bimodal dataset will allow future users to investigate
83 the potential advantages of using bimodal *versus* unimodal data for inner-speech recognition and will also contribute towards
84 the BCI development in the area of speech prostheses.

85 **Methods**

86 **Participants**

87 In order to identify participants for our study, we announced the study by distributing flyers describing the experimental
88 procedure and aim of the study, at the Lulea University of Technology, following a list of predefined inclusion and exclusion
89 criteria. In particular, the following inclusion criteria were followed: The current study aimed for an even gender distribution.
90 In order to homogenize the sample, only right-handed people were considered in the study. To facilitate communication during

91 data collection, which is mainly carried out by a non-Swedish-speaking person, primarily English speakers were consulted.
92 In the same manner, the following exclusion criteria were followed: If people have difficulty understanding or following
93 the instructions given at the time of preparation or if for some reason they were feeling uncomfortable during the magnetic
94 resonance imaging (MRI) or EEG examination, they were excluded from the study. All participants filled out an fMRI
95 pre-screening form in order to exclude people that should not undergo the experimental procedure (e.g., due to the presence
96 of metallic objects in their body, claustrophobia etc.). The study was approved by the *Swedish Ethical Review Authority*
97 (*Etikprövning myndigheten*, ID:2021-06710-01) (<https://etikprovningmyndigheten.se/>) in accordance with the Swedish Ethical
98 Review Act (SFS 2003:460). Ten participants filled out the questionnaire and as our ethical approval allowed only for a limited
99 amount of subjects, we decided to include only right-handed subjects covering both genders (at least 40% of each gender). As a
100 result, five healthy right-handed subjects aged 33-51 years, participated in this study (three females and two males). Detailed
101 information on the subjects in this study is shown in Table 1. None of these subjects were native English speakers.

102 All subjects followed the same experimental protocol for the two modalities. The acquisition of the EEG and fMRI
103 recording were performed sequentially followed the general approach of having an EEG recording followed by a fMRI
104 recording with at least one hour of relaxation in between. In this study, we refer to the subjects with the following naming
105 convention: sub-01, sub-02, sub-03, sub-04 and sub-05. Due to high fluctuations during the EEG recording the data from
106 sub-04 were excluded from this study. All subjects provided written consent to participate in the study and to publish this
dataset.

Table 1. Participant characteristics

Participant	Self-declared sex	Age	Handedness	Native language
sub-01	Male	33	Right	Hindi
sub-02	Male	35	Right	Bengali
sub-03	Female	51	Right	Greek
sub-04	Female	35	Right	Arabic
sub-05	Female	37	Right	Hindi

107

108 **fMRI hardware and setup**

109 The data were collected using a Siemens Magnetom Prisma MRI system (Siemens Healthineers, Erlangen, Germany), equipped
110 with a 20-channel head coil. The visual stimuli were presented during the fMRI recording from a computer to an Ultra HD
111 LCD display (NordicNeuroLab, Bergen, Norway). The screen was 88x48 cm (3,840x2,160 pixels at full resolution).

112 Anatomical images were acquired using a sagittal T1-weighted 3D magnetization-prepared rapid acquisition gradient echo
113 (MPRAGE) sequence with the following parameters: repetition time (TR) = 2.3 ms; echo time (TE) = 2.98 ms; inversion time
114 (TI) = 900 ms; flip angle = 9°; slices = 208; matrix size = 256x256; and voxel size = 1x1x1 mm. Right after the anatomical
115 scan, two field maps were obtained (A and B) with the following parameters: TR=662.0 ms, TE: A=4-92 ms, B=7.38 ms; and
116 voxel size = 3x3x2 mm. Next, functional maps were obtained using double-echo gradient echo imaging BOLD sequences
117 parallel to the bicommissural plane with the following parameters: TR = 2.16 s; TE = 30 ms; slices = 68; matrix size = 100x100
118 and voxel size = 2x2x2 mm.

119 **EEG hardware and setup**

120 The EEG data were acquired using the *BioSemi Active2* measuring system (BioSemi B.V., Amsterdam, Netherlands) with a
121 16-bit resolution and a sampling rate of 512 Hz. A BioSemi EEG head cap with 64 electrodes in pre-fixed electrode positions
122 and 6 external sensors was used. An appropriate cap size was selected for each participant by measuring his or her head
123 circumference from nasion toinion. We also ensured that the cap was properly centred with the C_z (Vertex) at the centre of the
124 head, namely, halfway between the nasion andinion and halfway between the two ears. *SignaGel* (Parker Laboratories BV,
125 Almelo, Netherlands) was applied to each electrode to provide electrode connectivity with the subject's head. All six external
126 electrodes (EXG1-EXG6) were placed using stickers. The locations of the six electrodes were as follows:

- 127 • EXG1: On the left mastoid behind the left ear
- 128 • EXG2: On the right mastoid behind the right ear
- 129 • EXG3: 1 cm to the left of the left eye (aligned to the centre of the eye)
- 130 • EXG4: 2 cm above the left eye (aligned to the centre of the eye)
- 131 • EXG5: 2 cm below the right eye (aligned to the centre of the eye)

- EXG6: 1 cm to the right of the right eye (aligned to the centre of the eye)

EEG data were recorded with ActiView software, which was also developed by BioSemi. ActiView enables verification of the electrode impedance as well as the overall quality of the incoming data. The impedance of each electrode was manually examined at the beginning of each recording session, to ensure that it was between $-20 \mu\text{V}$ and $20 \mu\text{V}$; any electrodes not within this range were adjusted before recording to ensure the correct impedance, by adding/removing some gel, moving the participant's hair underneath the electrode or wiggling the electrode. Lights in the room were dimmed to avoid subject's eye flickering due to the high contrast between the room and the visual display.

Experimental protocol

The overall experimental protocol consisted of two fMRI sessions and one EEG session and was performed over a period of 3 consecutive days. In this study, all EEG recordings were performed first, as the EEG setup can sometimes induce difficulties (e.g., achieving good electrode connectivity with the participant's head). During day-01, the EEG recordings of sub-01, sub-02 and sub-03 took place followed by the recordings of the first fMRI session. The majority of the fMRI recordings for the second session were performed during day-02; only the recordings of sub-05 were performed on day-03. There was always a relaxation period of at least one hour in between the recordings and proper time for a break to avoid participants' fatigue. The detailed EEG/fMRI schedule is illustrated in Figure 1.

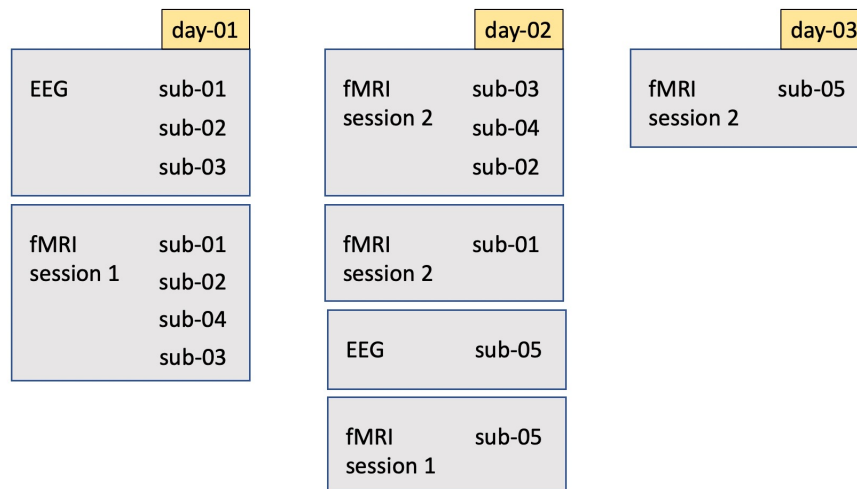


Figure 1. EEG/fMRI schedule - The overall experimental protocol performed over a period of 3 consecutive days. Day-01 contains the EEG recordings as well as the recordings of the first fMRI session of sub-01, sub-02, and sub-03. Note that also the fMRI session for sub-04 took place. Day-02 contains the fMRI recordings for session 2 of sub-01, sub-02, sub-03, and sub-04, the fMRI recordings for session 1 of sub-05 and the EEG recordings of sub-05. Day-03 contains the fMRI recordings for session 2 of sub-05. There was always a relaxation period of at least one hour in between the recordings and proper time for a break to avoid participants' fatigue.

The experimental protocol for both modalities (fMRI and EEG) was designed using E-Prime 3.0⁴⁶ and is illustrated in Figure 2. Huth *et al.*¹⁶ shows that semantically selective brain areas appear to be organised in the same manner across individuals and provides word frequency statistics for the text corpus employed. Based on the reference study, two categories, social and number, with four words each were selected. The two selected categories were mapped into different brain areas and the selected words appear to have a high word co-occurrence frequency. The social category contained the words *child, daughter, father, and wife*. The number category contained the words *four, three, ten, and six*. The textual representation of the words was presented randomly on the screen in front of the participant. There were a total of 2,080–2,200 fMRI volumes collected per subject, divided into two sessions. Each volume contained $100 \times 100 \times 68$ voxels. The EEG recordings provided a total of $320 \times 64 \times 1,024$ samples per subject.

fMRI procedure

The fMRI recordings consisted of two sessions performed over a period of three days. At the beginning of each session, written instructions for the experiment were presented on the screen until the participants informed the fMRI operator through an

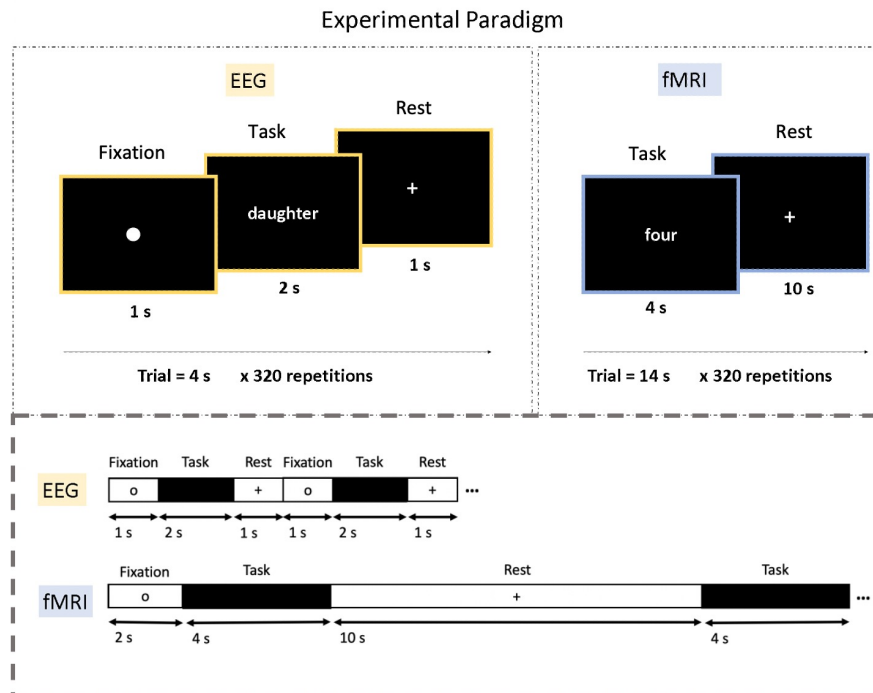


Figure 2. Experimental paradigm - The trial designs are depicted in the top part of the figure and the respected timelines for the trials are shown at the bottom. During the fMRI inner-speech task, participants were requested to think of the presented word as many times as possible. There were 320 trials in total, split into two sessions of 160 trials each. For the EEG recordings, there was only one session, and the presented stimulus was imagined only once for each inner-speech task interval. Note that the rest period for the fMRI protocol was longer than that for the EEG protocol

159 intercom that they are ready to proceed with the experiment. A fixation period of 2 s was followed, in which the participants
 160 were instructed to fixate their eyes on the centre of the screen. Then, each trial consisted of the inner-speech task (4 s)
 161 and a subsequent rest period (10 s). Eight different words were used for the inner-speech task, divided into 2 categories
 162 (social or number words), and there were 20 trials for each word in each session; thus, each session consisted of 160 trials.
 163 During the inner-speech task, the word stimulus was presented in white font against a black background for 4 s, and the
 164 participants were encouraged to repeat the given word in their minds as many times as possible (approximately 4 times) without
 165 any accompanying articulation or muscle movement (i.e., using their inner speech). The word stimuli were presented in a
 166 randomized order over the 160 trials. During the rest period, a white fixation cross was presented for 10 s, and the participants
 167 were allowed to relax and prepare for the next trial. The total duration of the recordings for the 320 repetitions was 74.6 min
 168 per participant.

169 EEG procedure

170 The EEG recordings consisted of one session with 40 trials per word, using the same stimuli as in the fMRI protocol, that
 171 was performed before the fMRI acquisition for all subjects but for sub-05 due to time constraints of the recording facility. At
 172 the beginning of the session, the written instructions for the experiment were presented on a screen to the subject until they
 173 pressed the spacebar to start the experiment. Each trial included fixation, task, and rest periods, with durations of 1 s, 2 s,
 174 and 1 s, respectively. During the fixation period, the participant was instructed to direct their gaze to the centre of the screen,
 175 where a small circular fixation point was located. During the task period, the word stimulus was presented for 2 s, and the participants
 176 were asked to repeat the stimulus in their minds without any accompanying articulation or muscle movement (i.e., using their
 177 inner speech). During the rest period, the participants were allowed to relax and prepare for the next trial. The total duration of
 178 the recording, which contained 320 repetitions, was 21.33 min per participant. Note that the rest period for the fMRI protocol
 179 was longer than that for the EEG protocol because the fMRI BOLD signal typically peaks approximately 5 s after stimulus
 180 onset and takes approximately 14 s to recover to baseline levels⁴⁷.

181 **fMRI Preprocessing**

182 The fMRI data were preprocessed with SPM12⁴⁸. First, spatial displacement maps were calculated for each session. These were
183 used for motion correction of the functional data. Slice-timing correction was performed as the fMRI data were acquired in an
184 interleaved order. Next, images were coregistered to the T1-weighted structural scan with a normalized mutual information cost
185 function. Prior to normalization, these images were used for within-subject classification.

186 To verify that neural activity related to inner speech and the two semantic categories (social and number words) was as
187 expected, further processing was conducted (see “fMRI activation – group level”). The origin was manually set to the anterior
188 commissure, followed by normalization to the Montreal Neurological Institute (MNI) space. Smoothing using an 8-mm
189 full-width at half-maximum (FWHM) Gaussian kernel was applied. We estimated a general linear model (GLM) convolved
190 with a canonical haemodynamic response function. The category regressors (social or number word) were time-locked to the
191 onset of its respective inner-speech word with a duration of 4 s. The rest of the regressors had durations of 10 s. Nuisance
192 variables, such as movement parameters calculated in the previous realignment step, were also included. This GLM enabled
193 investigation of the activation at the subject level; subsequently, a fixed effect analysis was applied to determine activation
194 at the group level. The planned comparisons included inner speech and rest (inner speech – rest) and the stimulus category
195 (number word – social word; social word – number word). For all analyses, the extent cluster threshold was $^KE > 20$ with a
196 familywise error (FWE) correction of $p < 0.05$ at the voxel level.

197 **EEG preprocessing**

198 In the current work, we utilized EEGLAB⁴⁹ to preprocess the EEG data. EEGLAB is a MATLAB toolbox for processing
199 continuous and event-related EEG, MEG, and other electrophysiological data. The toolbox has features such as independent
200 component analysis (ICA), time/frequency analysis, artefact rejection, event-related statistics, and several useful visualization
201 modes for averaged and single-trial data.

202 The raw BioSemi EEG data in .bdf format were imported to EEGLAB using reference channel 48 (Cz). A multitude of
203 internal and environmental causes can generate temporal drifts, which change over time and across the electrodes. To reduce
204 the impact of such variances, it is usual practice to perform a so-called baseline correction. In this study, baseline correction
205 was applied using a zero-phase finite impulse response (FIR) high-pass filter at 0.1 Hz. Low-frequency and high-frequency
206 signals, which are commonly caused by environmental/muscle noise in scalp EEG and are not usually the focus of analysis,
207 were filtered out.

208 Noise below and above a given frequency was retained using low-pass and high-pass filtering. Here, we applied zero-phase
209 finite impulse response (FIR) bandpass filtering with 0.1 Hz (lower edge) and 50 Hz (higher edge) boundaries of the frequency
210 bandpass, eliminating the requirement for a notch filter. Rereferencing facilitates data cleaning by providing an estimate
211 of physiological noise at baseline. In this study, rereferencing was performed using the average reference to Cz, excluding
212 channels 65-70 (the mastoid and ocular electrodes); averaging referencing was chosen over rereferencing from the mastoid
213 electrodes to guard against introducing any signal artifacts which may have resulted from differences in placement of the
214 external electrodes between participants (as per, for example, our decision to disregard the data from subject 4 (sub-04), to
215 ensure overall data integrity).

216 Channels were manually inspected, and bad channels were rejected and not interpolated. Time-locked epochs were extracted
217 using start-stop limits fixed within the interval [0, 2 s]. ICA can be used to identify data segments strongly influenced by
218 motor-related artefacts, such as eye blinking and movement of the jaw, neck, arm, or upper back, for removal. Figure 3
219 illustrates two out of the 64 ICA components. In this study, we examined the topography as well as the spectrogram and
220 frequency variation to decide whether a component should be retained. In examining the topographies, high activity in the
221 far-frontal projections is a strong indicator of electrooculography (EOG) artifacts; in the spectra, decreasing power with a slope
222 that is more shallow and spread more evenly over the frequency range is also a strong indicator of an EOG artifact: taken
223 together (along with the ocular reference channels, 67-70, which serve to provide the EOG signal pattern that the independent
224 components are matched against) we reliably identified artifact-related independent components to zero-out from the data, as
225 part of a manual inspection and cleaning process that is often more reliable than algorithmic methods relying on peak-to-peak
226 signal information, which may vary greatly between subjects.

227 Finally, we extracted epochs according to the *time-locking event*. We performed this process manually, with the epoch limit
228 [0,2 s], this interval encapsulated the main activity.

229 **Data Records**

230 The anonymized EEG and fMRI data of the four subjects are available in *Brain Imaging Data Structure* (BIDS) format
231 (<https://bids-specification.readthedocs.io/en/stable/>) at the OpenNeuro repository⁵⁰. The data for each subject are organized into
232 three sessions: two for the fMRI modality (ses-01 and ses-02) and one for the EEG modality (ses-EEG), as shown in Figure 4.
233 A total of 2,560 trials are provided in this dataset, out of which half (1,280) were with fMRI and half were with EEG. There

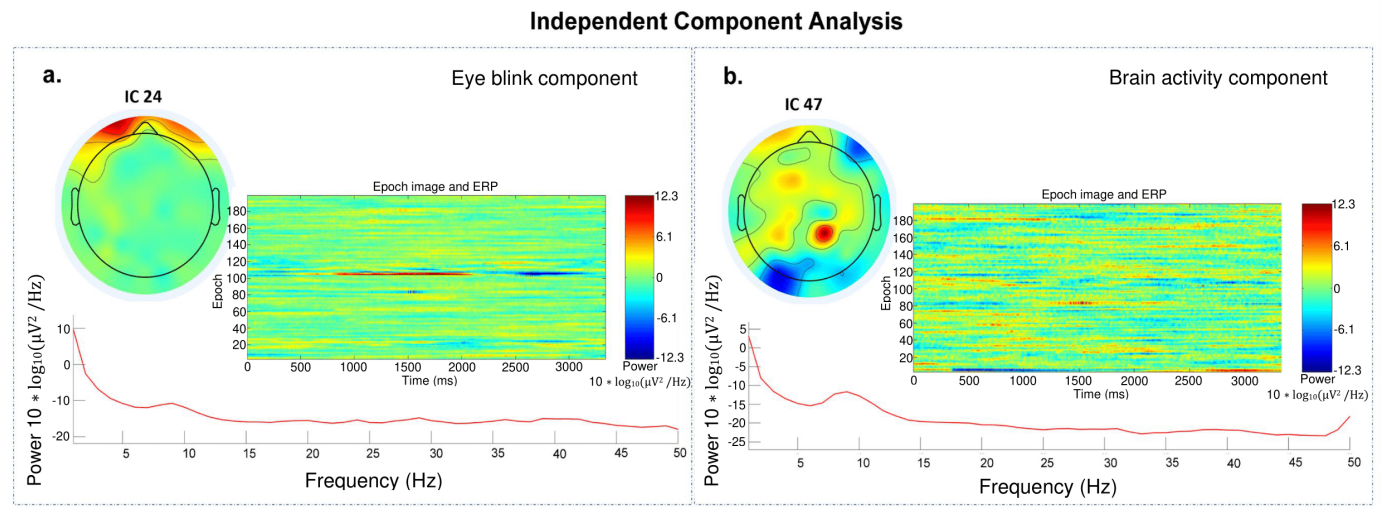


Figure 3. Components decomposed by ICA, showing eye blinks and brain activity. Top left: topography map illustrating the projection of the independent component activity. Center: event-related potentials of the independent component and its associated power, per epoch. Bottom: spectrum of the independent component.

234 are 4 directories, one for each subject (i.e., sub-01, sub-02, sub-03, and sub-05). The data from sub-04 were deemed unfit for
235 use and thus were not made available.

236 **fMRI.** All Digital Imaging and Communications in Medicine (DICOM) files with fMRI data were converted into
237 Neuroimaging Informatics Technology Initiative (NIFTI) format using *MRICroGL v1.2.0211006*
238 (<https://www.nitrc.org/plugins/mwiki/index.php/mricrogl>) and then organized into BIDS format. Regarding file organization,
239 each individual subject folder contains the three sessions described above. The ses-01 folder contains three subfolders that
240 include the anatomical (anat), field map (fmap), and functional (func) images. The ses-02 folder contains two subfolders,
241 namely, fmap and func, as anatomical scans were not performed in session 2 for any of the subjects. Each .nifti file in the
242 dataset is accompanied by the corresponding .json file. The anatomical image from session 1 of each subject consists of
243 the anatomical scan with file names in the following format: sub-XX-YY-T1W, where XX denotes the subject ID and YY
244 denotes the session ID. The fmap folder in each session of a subject consists of three .nifti files and their corresponding
245 .json files. Two of the .nifti files are for magnitude, and one is for phase difference. The two magnitude files are named
246 with the following format: sub-XX-YY-magnitudeZ, where XX denotes the subject ID, YY denotes the session ID, and Z
247 takes the value 1 for $TE1 = 4.92ms$ and 2 for $TE2 = 7.38ms$. The .nifti file for the phase difference image is named with the
248 following format: sub-XX-ses-YY-phasediff, where XX denotes the subject ID and YY denotes the session ID. The functional
249 data are made available in the func folder, where the .nifti file and its corresponding .json file have the following format:
250 sub-XX-ses-YY-task-inner-bold, where XX denotes the subject ID and YY denotes the session ID. The task event file is also
251 available as a .tsv file named sub-XX-ses-YY-task-inner-events, where XX denotes the subject ID and YY denotes the session
252 ID in the corresponding func folders.

253 **EEG.** The EEG data were collected in one session, and raw EEG files are available in the ses-EEG folder for each subject.
254 The raw EEG data are available in .bdf format. The .bdf file was exported using EEGLAB software v2021.1, and the sampling
255 rate was 512. Each event and its corresponding ID and description are presented in Table 2. The different channel data are
256 provided in 72 rows (64 EEG, 8 external). Out of 8 external electrodes, only six were connected; specifically, the CMS and
257 DRL electrodes were not recorded.

258 The task events are provided in a .tsv file for corresponding subjects in the respective ses-EEG folders. The continuous
259 recordings of the 64 EEG channels, the 6 external channels, and the labeled events were included in the saved files.

260 Technical Validation

261 EEG

262 An event related potential (ERP) is the measured brain activity in response to a stimulus, therefore suitable for verifying the
263 technical validity of the data. Although the entire dataset is available at the OpenNeuro repository⁵⁰, in this work, we provide
264 the ERP activity for two subjects in Figure 5, as an example. In order to represent all available genders in this study, sub-01

EventID	Description
1	fixation
2	rest
111	child
112	daughter
113	father
114	wife
125	four
126	three
127	ten
128	six

Table 2. Event IDs and their accompanying descriptions.

265 (male) and sub-03 (female) were selected.

266 From both plots, it can be observed that more pronounced potential deflections occur after stimulus presentation (i.e.,
267 after $t=0$ ms); however, a small range of deflection can also be noticed within the two other periods (rest and fixation); the
268 presentation of new visual stimuli to the subjects, to signal the start of each period within each trail, has resulted in these evoked
269 responses (so-called fixation-onset ERPs⁵¹).

270 The activity at 235 ms and 285 ms for sub-01, and at 250 ms and 320 ms for sub-03 indicate prominent brain activity
271 stimulus onset. Specifically, sub-01 displayed high activity, linked to the frontal lobe, during the first 500 ms compared to
272 the low activity of sub-03 in the same period. This difference might be a result of eye movements by sub-01. Interestingly,
273 for sub-03, the plotted waves were close to the baseline during the fixation period, indicating low brain activity associated
274 with gaze at the fixation circle. Data from both subjects followed similar pattern during the inner-speech task (0-500 ms). As
275 shown in Figure 5, strong positive and negative deflections occurred during 0-500 ms, which indicate the evoked response upon
276 presentation of the visual stimulus, and increased brain activity during the performance of the inner-speech task. These evoked
277 responses indicate strong P300 and N400 components, which are observed in similar trials for imagined speech⁵² and validate
278 the inner-speech data that have been recorded under our experimental protocol.

279 Next, to provide a more detailed analysis of the activated brain areas, we generated topological maps (after ICA decomposi-
280 tion). Figure 6 depicts the activation in response to stimuli in the two semantic categories (number or social words) for all
281 subjects in topological maps. As shown in the figure, it appears that these activities were mainly dominated by frontal and
282 central regions. Notably, the activity in response to all stimuli (eight words) is shown in the topological maps in Figure 7. In
283 this figure, 4 ICs with high brain activity are shown for all words. For a specific IC, regions were differently activated for each
284 of the eight words. The topographic projections of each word illustrate the average difference in brain activity between the
285 inner-speech task of each word; the variance between these projections confirms the subject's different activation regions, both
286 between and within our semantic categories, which further validates the data.

287 **fMRI activation - group level**

288 In this study, the group level analyses were conducted to verify that the inner-speech task activated neural regions connected to
289 inner speech. As expected, the inner-speech task activated language- and orthographic-related regions when compared with
290 the baseline rest condition. The increased activity during inner speech (see Figure 8(a) and Table 3) is indicated by average
291 BOLD activation displaying significant activation in areas directly related to language processing, including Wernicke's area
292 (Brodmann's area (BA) 22) in the left hemisphere and Broca's area and surrounding regions. Further activation was found in
293 the left supramarginal gyrus, which (alongside the pars opercularis) has been implicated in inner speech⁵³, and the angular
294 gyrus, which is related to semantic processing^{54,55}. Areas of high activation also included visual processing regions, such as the
295 bilateral secondary visual cortex and the right frontal eye fields, and orbitofrontal area. These regions likely relate to processing
296 of visual word forms, as the word cue was presented orthographically. Not surprisingly, motor regions, including the primary
297 motor cortex and premotor and supplementary motor cortices, were activated by the inner-speech task. Motor activity still
298 occurs during inner-speech⁵⁶, albeit at reduced activation levels compared to outer speech (spoken aloud)⁵⁷. These findings
299 support the reliability of the data as they indicate that the inner-speech task activated language, orthographic, and motor related
300 regions.

301 Comparison of the two semantic categories (social vs. number words) revealed that social words elicited more activation
302 than number words in the bilateral secondary visual cortex and the right primary visual cortex (see Table 4 and Figure 8(b)).
303 No areas showed significantly higher activation for number words compared to social words.

304 **fMRI activation - individual subjects**

305 Decoding studies are often conducted within rather than between subjects due to the large extent of individual variance in
306 neural anatomy and functional activity. Therefore, we provided subject-level results to enable researchers to select among
307 subjects based on brain activation profiles. As seen in Figure 9, the results are consistent across subjects.

308 **fMRI framewise displacement**

309 Motion-related artifacts can compromise data quality. Frames that are contaminated with motion above a certain threshold can
310 be rejected by calculating head motion artifacts through framewise displacement (FD). FD is an overall estimate of movement
311 over time for each subject, which incorporates subtle in-scanner movements. We calculated the FD for each subject and session
312 in Nipype, according to Power *et al.*⁵⁸. The average FD (in mm) across frames for each subject was as follows: sub-01, session
313 1=0.13 and session 2=0.14; sub-02, session 1=0.15 and session 2=0.14; sub-03, session 1=0.11 and session 2=0.1; and sub-05,
314 session 1=0.2 and session 2=0.22; see Figure 10. There was rarely motion exceeding the size of one voxel ($2 \times 2 \times 2$ mm).
315 The analysis also showed that all subjects had a mean FD under 0.25 mm; however, researchers may choose to omit specific
316 volumes with FD values higher than 0.5 mm.

317 **Code Availability**

318 The code used to preprocess the EEG and fMRI data as well as the two stimulation protocols (one for each modality) are
319 publicly available at: https://github.com/LTU-Machine-Learning/Inner_Speech_EEG_FMRI.

320 **References**

- 321 1. He, B., Yuan, H., Meng, J. & Gao, S. Brain–computer interfaces. In *Neural engineering*, 131–183 (Springer, 2020).
- 322 2. Abiri, R., Borhani, S., Sellers, E. W., Jiang, Y. & Zhao, X. A comprehensive review of eeg-based brain–computer interface
323 paradigms. *J. neural engineering* **16**, 011001 (2019).
- 324 3. Alderson-Day, B. & Fernyhough, C. Inner speech: development, cognitive functions, phenomenology, and neurobiology.
325 *Psychol. bulletin* **141**, 931 (2015).
- 326 4. Whitford, T. J. *et al.* Neurophysiological evidence of efference copies to inner speech. *Elife* **6**, e28197 (2017).
- 327 5. Smallwood, J. & Schooler, J. W. The science of mind wandering: empirically navigating the stream of consciousness.
328 *Annu. review psychology* **66**, 487–518 (2015).
- 329 6. Filik, R. & Barber, E. Inner speech during silent reading reflects the reader’s regional accent. *PloS one* **6**, e25782 (2011).
- 330 7. Angrick, M. *et al.* Real-time synthesis of imagined speech processes from minimally invasive recordings of neural activity.
331 *Commun. biology* **4**, 1–10 (2021).
- 332 8. Dash, D., Ferrari, P., Berstis, K. & Wang, J. Imagined, intended, and spoken speech envelope synthesis from neuromagnetic
333 signals. In *International Conference on Speech and Computer*, 134–145 (Springer, 2021).
- 334 9. McGuire, P. *et al.* The neural correlates of inner speech and auditory verbal imagery in schizophrenia: relationship to
335 auditory verbal hallucinations. *The Br. J. Psychiatry* **169**, 148–159 (1996).
- 336 10. Barber, L., Reniers, R. & Uptegrove, R. A review of functional and structural neuroimaging studies to investigate the
337 inner speech model of auditory verbal hallucinations in schizophrenia. *Transl. psychiatry* **11**, 1–12 (2021).
- 338 11. Perrone-Bertolotti, M., Rapin, L., Lachaux, J.-P., Baciú, M. & Loevenbruck, H. What is that little voice inside my head?
339 inner speech phenomenology, its role in cognitive performance, and its relation to self-monitoring. *Behav. brain research*
340 **261**, 220–239 (2014).
- 341 12. Skeide, M. A. & Friederici, A. D. The ontogeny of the cortical language network. *Nat. Rev. Neurosci.* **17**, 323–332 (2016).
- 342 13. Blank, S. C., Scott, S. K., Murphy, K., Warburton, E. & Wise, R. J. Speech production: Wernicke, broca and beyond. *Brain*
343 **125**, 1829–1838 (2002).
- 344 14. Sahin, N. T. *et al.* Sequential processing of lexical, grammatical, and phonological information within broca’s area. *Science*
345 **326**, 445–449 (2009).
- 346 15. Mitchell, T. M. *et al.* Predicting human brain activity associated with the meanings of nouns. *science* **320**, 1191–1195
347 (2008).
- 348 16. Huth, A. G. *et al.* Natural speech reveals the semantic maps that tile human cerebral cortex. *Nature* **532**, 453–458 (2016).

- 349 **17.** Rueckl, J. G. *et al.* Universal brain signature of proficient reading: Evidence from four contrasting languages. *Proc. Natl.*
350 *Acad. Sci.* **112**, 15510–15515 (2015).
- 351 **18.** Wilson, J. A., Felton, E. A., Garell, P. C., Schalk, G. & Williams, J. C. Ecog factors underlying multimodal control of a
352 brain-computer interface. *IEEE transactions on neural systems rehabilitation engineering* **14**, 246–250 (2006).
- 353 **19.** Fabiani, G. E., McFarland, D. J., Wolpaw, J. R. & Pfurtscheller, G. Conversion of eeg activity into cursor movement by a
354 brain-computer interface (bci). *IEEE transactions on neural systems rehabilitation engineering* **12**, 331–338 (2004).
- 355 **20.** Andersson, P. *et al.* Real-time decoding of brain responses to visuospatial attention using 7t fmri. *PloS one* **6**, e27638
356 (2011).
- 357 **21.** Kamavuako, E. N., Sheikh, U. A., Gilani, S. O., Jamil, M. & Niazi, I. K. Classification of overt and covert speech for
358 near-infrared spectroscopy-based brain computer interface. *Sensors* **18**, 2989 (2018).
- 359 **22.** Rezazadeh Sereshkeh, A. *et al.* Development of a ternary hybrid fNIRS-EEG brain-computer interface based on imagined
360 speech. *Brain-Computer Interfaces* **6**, 128–140 (2019).
- 361 **23.** Dash, D. *et al.* Meg sensor selection for neural speech decoding. *IEEE Access* **8**, 182320–182337 (2020).
- 362 **24.** Dash, D. *et al.* Decoding imagined and spoken phrases from non-invasive neural (MEG) signals. *Front. neuroscience* **14**
363 (2020).
- 364 **25.** Aggarwal, S. & Chugh, N. Signal processing techniques for motor imagery brain computer interface: A review. *Array* **1**,
365 100003 (2019).
- 366 **26.** Chholak, P. *et al.* Visual and kinesthetic modes affect motor imagery classification in untrained subjects. *Sci. reports* **9**,
367 1–12 (2019).
- 368 **27.** Donchin, E., Spencer, K. M. & Wijesinghe, R. The mental prosthesis: assessing the speed of a p300-based brain-computer
369 interface. *IEEE transactions on rehabilitation engineering* **8**, 174–179 (2000).
- 370 **28.** da Silva-Sauer, L., Valero-Aguayo, L., de la Torre-Luque, A., Ron-Angevin, R. & Varona-Moya, S. Concentration on
371 performance with p300-based bci systems: A matter of interface features. *Appl. ergonomics* **52**, 325–332 (2016).
- 372 **29.** Herff, C. *et al.* Brain-to-text: decoding spoken phrases from phone representations in the brain. *Front. neuroscience* **9**, 217
373 (2015).
- 374 **30.** Martin, S., Iturrate, I., Millán, J. d. R., Knight, R. T. & Pasley, B. N. Decoding inner speech using electrocorticography:
375 Progress and challenges toward a speech prosthesis. *Front. neuroscience* **12**, 422 (2018).
- 376 **31.** Panachakel, J. T. & Ramakrishnan, A. G. Decoding covert speech from eeg-a comprehensive review. *Front. Neurosci.* 392
377 (2021).
- 378 **32.** Cooney, C., Folli, R. & Coyle, D. Optimizing layers improves CNN generalization and transfer learning for imagined
379 speech decoding from EEG. In *2019 IEEE International Conference on Systems, Man and Cybernetics (SMC)*, 1311–1316
380 (IEEE, 2019).
- 381 **33.** Schirrmester, R. T. *et al.* Deep learning with convolutional neural networks for EEG decoding and visualization. *Hum.*
382 *brain mapping* **38**, 5391–5420 (2017).
- 383 **34.** van den Berg, B., van Donkelaar, S. & Alimardani, M. Inner speech classification using eeg signals: A deep learning
384 approach. In *2021 IEEE 2nd International Conference on Human-Machine Systems (ICHMS)*, 1–4 (IEEE, 2021).
- 385 **35.** Yoo, S.-S. *et al.* Brain-computer interface using fmri: spatial navigation by thoughts. *Neuroreport* **15**, 1591–1595 (2004).
- 386 **36.** Zhao, S. & Rudzicz, F. Classifying phonological categories in imagined and articulated speech. In *2015 IEEE International*
387 *Conference on Acoustics, Speech and Signal Processing (ICASSP)*, 992–996 (IEEE, 2015).
- 388 **37.** Coretto, G. A. P., Gareis, I. E. & Rufiner, H. L. Open access database of EEG signals recorded during imagined speech. In
389 *12th International Symposium on Medical Information Processing and Analysis*, vol. 10160, 1016002 (2017).
- 390 **38.** Nguyen, C. H. *et al.* Inferring imagined speech using EEG signals: a new approach using Riemannian manifold features. *J.*
391 *neural engineering* **15**, 016002 (2017).
- 392 **39.** Ferreira, C. *et al.* Inner speech in portuguese: Acquisition methods, database and first results. In *International Conference*
393 *on Computational Processing of the Portuguese Language*, 438–447 (Springer, 2018).
- 394 **40.** Nieto, N., Peterson, V., Rufiner, H. L., Kamienkowski, J. E. & Spies, R. Thinking out loud, an open-access eeg-based bci
395 dataset for inner speech recognition. *Sci. Data* **9**, 1–17 (2022).

- 396 **41.** Perronnet, L. *et al.* Unimodal versus bimodal eeg-fmri neurofeedback of a motor imagery task. *Front. Hum. Neurosci.* **11**,
397 193 (2017).
- 398 **42.** Cooney, C., Folli, R. & Coyle, D. A bimodal deep learning architecture for eeg-fmri decoding of overt and imagined
399 speech. *IEEE Transactions on Biomed. Eng.* (2021).
- 400 **43.** Lioi, G. *et al.* Simultaneous eeg-fmri during a neurofeedback task, a brain imaging dataset for multimodal data integration.
401 *Sci. data* **7**, 1–15 (2020).
- 402 **44.** Berezutskaya, J. *et al.* Open multimodal ieeg-fmri dataset from naturalistic stimulation with a short audiovisual film. *Sci.*
403 *Data* **9**, 1–13 (2022).
- 404 **45.** Scrivener, C. L. When is simultaneous recording necessary? a guide for researchers considering combined eeg-fmri. *Front.*
405 *Neurosci.* **15**, 774 (2021).
- 406 **46.** Schneider, W., Eschman, A. & Zuccolotto, A. E-prime (version 2.0). *Comput. software manual*. Pittsburgh, PA: Psychol.
407 *Softw. Tools Inc* (2002).
- 408 **47.** Dale, A. M. & Buckner, R. L. Selective averaging of rapidly presented individual trials using fmri. *Hum. brain mapping* **5**,
409 329–340 (1997).
- 410 **48.** Penny, W. D., Friston, K. J., Ashburner, J. T., Kiebel, S. J. & Nichols, T. E. *Statistical parametric mapping: the analysis of*
411 *functional brain images* (Elsevier, 2011).
- 412 **49.** Delorme, A. & Makeig, S. EEGLAB: an open source toolbox for analysis of single-trial EEG dynamics including
413 independent component analysis. *J. neuroscience methods* **134**, 9–21 (2004).
- 414 **50.** Liwicki, F. *et al.* "Bimodal dataset on Inner speech". *OpenNeuro* <https://doi:10.18112/openneuro.ds004197.v1.0.2> (2022).
- 415 **51.** Katz, C. N. *et al.* Differential generation of saccade, fixation, and image-onset event-related potentials in the human mesial
416 temporal lobe. *Cereb. Cortex* **30**, 5502–5516 (2020).
- 417 **52.** Villena-González, M., López, V. & Rodríguez, E. Orienting attention to visual or verbal/auditory imagery differentially
418 impairs the processing of visual stimuli. *Neuroimage* **132**, 71–78 (2016).
- 419 **53.** Geva, S. *et al.* The neural correlates of inner speech defined by voxel-based lesion–symptom mapping. *Brain* **134**,
420 3071–3082 (2011).
- 421 **54.** Devlin, J. T., Matthews, P. M. & Rushworth, M. F. Semantic processing in the left inferior prefrontal cortex: a combined
422 functional magnetic resonance imaging and transcranial magnetic stimulation study. *J. cognitive neuroscience* **15**, 71–84
423 (2003).
- 424 **55.** Hartwigsen, G. *et al.* Dissociating parieto-frontal networks for phonological and semantic word decisions: a condition-and-
425 perturb tms study. *Cereb. cortex* **26**, 2590–2601 (2016).
- 426 **56.** Loevenbruck, H. *et al.* Neural correlates of inner speaking, imitating and hearing: an fmri study. In *ICPhS 2019-19th*
427 *International Congress of Phonetic Sciences* (2019).
- 428 **57.** Palmer, E. D. *et al.* An event-related fmri study of overt and covert word stem completion. *Neuroimage* **14**, 182–193
429 (2001).
- 430 **58.** Power, J. D., Barnes, K. A., Snyder, A. Z., Schlaggar, B. L. & Petersen, S. E. Spurious but systematic correlations in
431 functional connectivity mri networks arise from subject motion. *Neuroimage* **59**, 2142–2154 (2012).

432 **Acknowledgements**

433 This research was funded by the Grants for Excellent Research Projects Proposals of SRT.ai 2022. We would like to thank
434 the Stockholm University Brain Imaging Centre (SUBIC) and, in particular, Rita Almeida and Patrik Andersson for giving us
435 access to their facilities and for supporting us in this endeavour. We thank Petter Kallioinen and Christoffer Schiehe-Forbes
436 for their valuable support during the acquisition of EEG data. Finally, we would also like to thank all participants for taking part in
437 this study.

438 **Author contributions statement**

439 F.S.L.: project conception, experimental design, data acquisition, writing, and finalizing the manuscript. V.G.: conducted the
440 processing part of the EEG data, and writing EEG-related sections of the manuscript. R.S.: processing of EEG data and writing
441 EEG-related sections of the manuscript. K.D.: processing and technical validation of fMRI data and writing all sections of
442 the manuscript. N.A.: review of all sections of the manuscript. S.R.: data management and availability. S.W.: advised the

443 pipeline for EEG data processing and validation, processing results, and writing related sections of the manuscript. H.W.:
444 designed the pipeline for processing and technical validation of fMRI data as well as writing all sections of the manuscript.
445 M.L.: advised the experimental and research design and the writing of the manuscript. J.E.: advised the experimental design,
446 technical validation of fMRI data, and writing of the manuscript. All authors reviewed the manuscript.

447 **Competing Interests**

448 The authors declare that they have no competing interests.

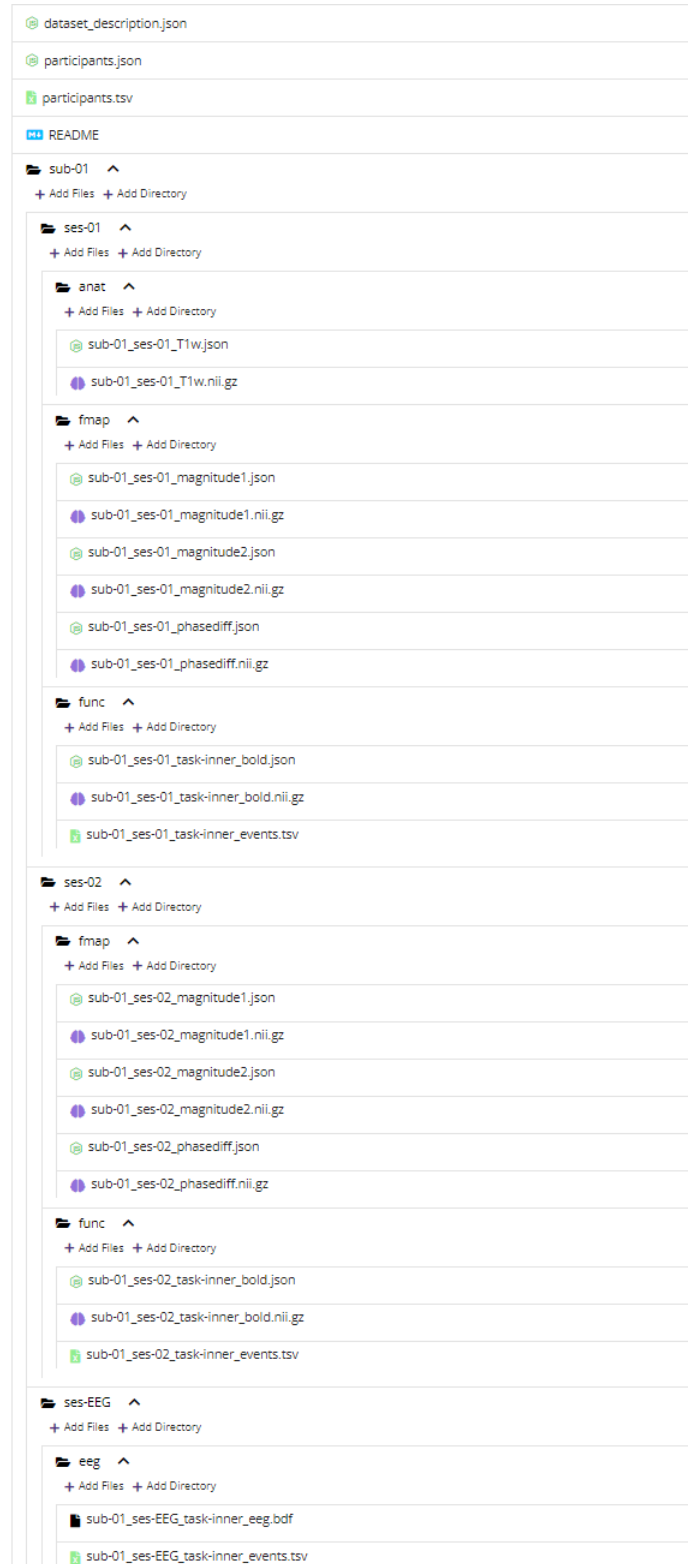


Figure 4. Example dataset structure for subject 1 (sub-01). The data are organized into three sessions: two for the fMRI modality (ses-01 and ses-02) and one for the EEG modality (ses-EEG).

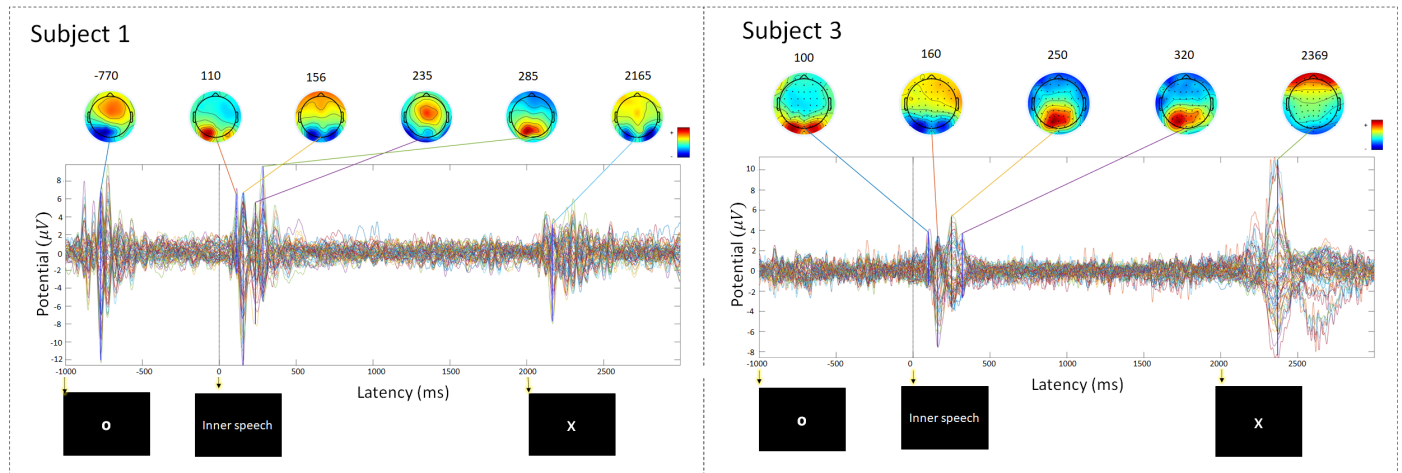


Figure 5. Plot of event-related potentials and topographical maps of activity for subjects 1 (sub-01) and 3 (sub-03). Both plots are created from preprocessed data by averaging over 320 trials for each subject. The 64 coloured waves correspond to the 64 EEG channels. The time axis shows the duration of a single trial and corresponds to a total duration of 4,000 ms. Notably, the time axis starts from a negative value of $t = -1,000$ ms, which corresponds to the 1,000 ms fixation period at the beginning of a trial. The times marked with arrows indicate the start of the fixation, inner-speech task, and rest periods (at -1,000 ms, 0 ms and 2,000 ms respectively).

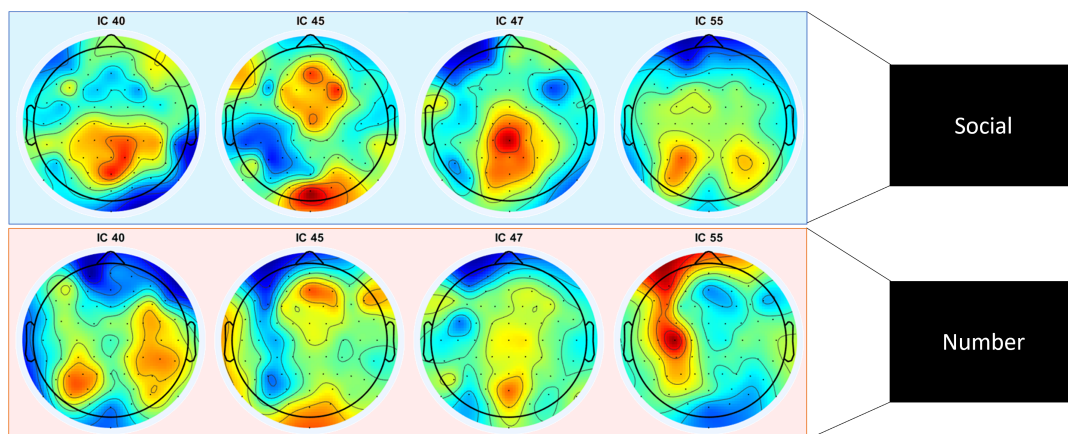


Figure 6. Topological maps (averaged over all subjects) corresponding to stimuli from the number and social categories for components 40, 45, 47, and 55.

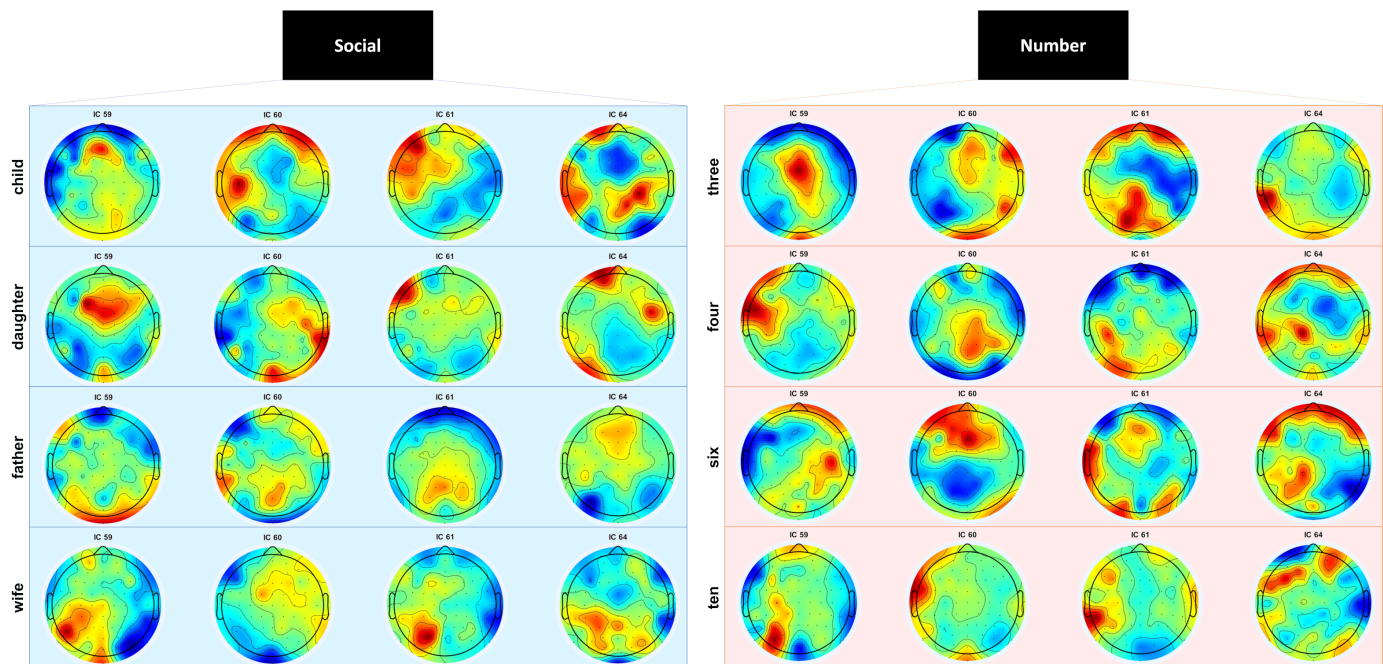


Figure 7. Topological maps (averaged over all subjects) for each stimulus in the number and social categories for components 59, 60, 61, and 64.

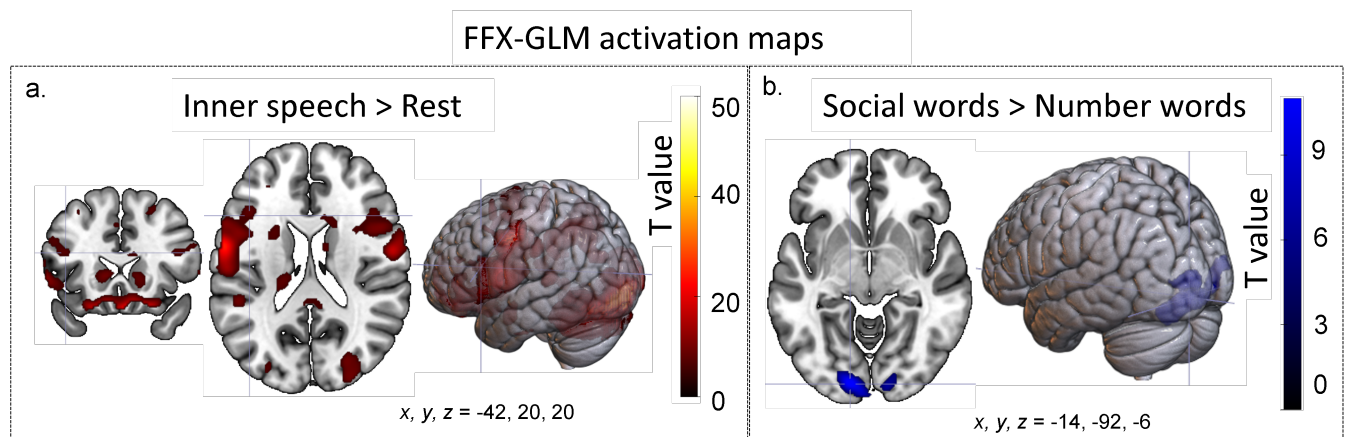


Figure 8. Activation map generated from fixed effects (FFX) and the general linear model (GLM) for the following: a. areas more highly activated during the inner-speech task than the resting condition (number and social words combined) – this slice is selected to highlight activation in Broca’s area (coordinates: -42, 20, 20), and b. areas more highly activated by social words than number words – this slice is selected to highlight activation in the secondary visual cortex (coordinates: 14, -92, -6). An increase in activation was found for the reverse contrast (i.e., increased activation for number words over social words).

Table 3. Areas with increased activation during inner speech relative to baseline (the rest condition). Coordinates are in Montreal Neurological Institute (MNI) space. *BA* = Brodmann's Area, *Hemi* = hemisphere, KE = cluster size. The cluster threshold was set to 20, with family-wise error (FWE)-adjusted $p < 0.05$

Anatomical area	BA	Hemi	(x y z)	KE	Peak T Value	ZE
Secondary visual cortex	18	L	-22, -96, -6	10470	54.5	Inf
	-	R	22, -98, 2	-	41.4	Inf
	-	R	30, -92, 2	-	38.89	Inf
Primary motor cortex	4	L	-50, -12, 44	1595	23.16	Inf
	-	L	50, -6, 42	-	16.57	Inf
	-	L	-56, -4, 20	-	14.77	Inf
Premotor cortex/supplementary motor area	6	R	50, -6, 42	1515	20.59	Inf
	6	R	50, -6, 56	-	15.37	Inf
Primary motor cortex	4	R	58, -4, 30	-	9.98	Inf
Praecuneus/superior parietal lobule	7	L	-24, -58, 54	2534	15.54	Inf
Supramarginal gyrus	40	L	-36, -40, 44	-	13.66	Inf
Praecuneus/superior parietal lobule	7	L	-20, -68, 44	-	11.32	Inf
Anterior prefrontal cortex	10	R	28, 64, 8	476	15.43	Inf
	-	R	18, 64, 8	-	15.34	Inf
	-	L	-22, 60, 2	-	14.22	Inf
Premotor cortex/supplementary motor area	6	L	-6, -4, 68	965	13.87	Inf
	-	L	-4, 2, 62	-	12.59	Inf
	-	R	6, -2, 70	-	9.36	Inf
Pars orbitalis	47	R	24, 18, -20	60	10.4	Inf
	-	R	32, 28, -18	-	6.82	6.81
Praecuneus/superior parietal lobule	7	R	30, -46, 44	1394	10.32	Inf
Angular gyrus	39	R	30, -62, 44	-	10.12	Inf
	-	R	28, -52, 52	-	9.8	Inf
Pars orbitalis	47	L	-22, 20, -22	121	9.83	Inf
	-	-	-18, 10, -22	-	7.5	7.48
	-	-	-14, 12, -14	-	5.72	5.72
Pars orbitalis	47	R	44, 30, -14	51	9.67	Inf
Basal ganglia	-	L	-12, 20, 2	1044	9.39	Inf
	-	L	-24, 6, 0	-	7.3	7.3
	-	L	-18, 12, -4	-	7.1	7.3
Premotor cortex/supplementary motor area	6	L	-48, 2, 4	107	8.02	Inf
Superior temporal gyrus	22	L	-52, -40, 16	93	7.88	Inf
Inferior frontal gyrus: pars triangularis	45	L	-48, 22, -2	45	7.46	7.45
Orbitofrontal area	11	R	4, 26, -12	80	6.77	6.76
Primary motor cortex	4	L	-16, -26, 64	65	6.58	6.57
Ventral anterior cingulate	24	R	8, 18, 20	177	6.33	6.33
Inferior frontal gyrus: pars opercularis	44	L	-42, 20, 20	93	6.31	6.3
Global pallidus	-	R	22, -4, 4	31	5.76	5.75
Frontal eye fields	8	R	10, 16, 34	72	5.74	5.73
Pars opercularis	44	R	50, 12, 20	32	5.57	5.56
Thalamus	-	L	-8, -20, 8	35	5.5	5.5

Table 4. Areas with increased activation for social words relative to number words during inner speech, i.e. the baseline. Coordinates are in Montreal Neurological Institute (MNI) space. *BA* = Brodmann's area, *Hemi* = hemisphere, *^KE* = cluster size. The cluster threshold was set to 20. The family-wise error (FWE) was adjusted to $p < 0.05$

Anatomical area	BA	Hemi	(x y z)	^K E	Peak T Value	^Z E
Secondary visual cortex	18	L	-14, -92, -6	1043	11.91	Inf
	-	-	-20, -98, 8	-	7.37	7.36
	-	-	-36, -90, 10	-	4.75	4.75
Primary visual cortex	17	R	12, -94, -4	321	7.85	7.83
Secondary visual cortex	18	R	26, -96, 12	-	6.08	6.08

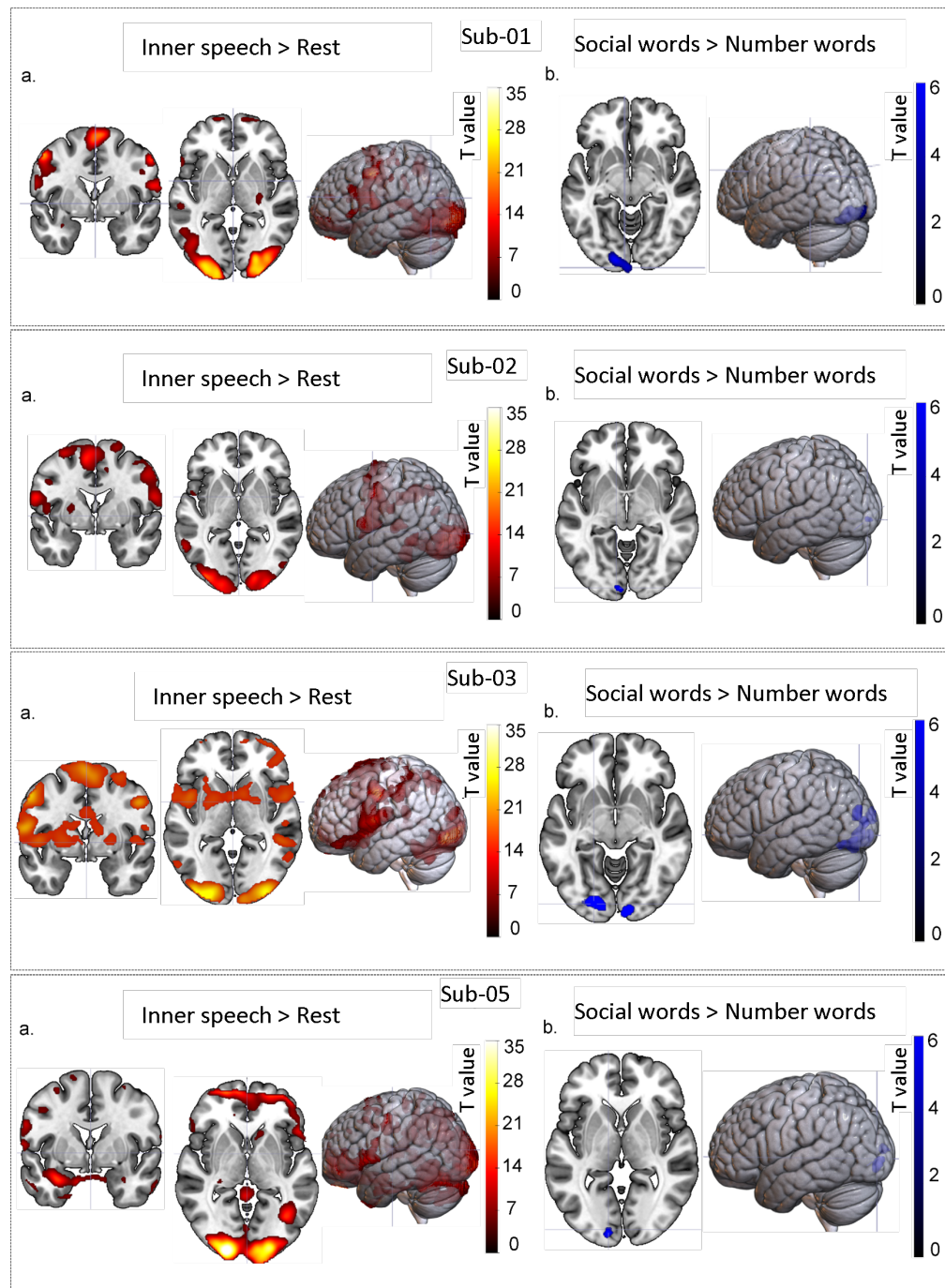


Figure 9. BOLD signals of each subject. **a.** Area more highly activated during the inner-speech task in the rest condition (numbers and social words combined). **b.** Areas more highly activated by social words than number words (no areas were more highly activated by number words than social words).

framewise displacement (FD)

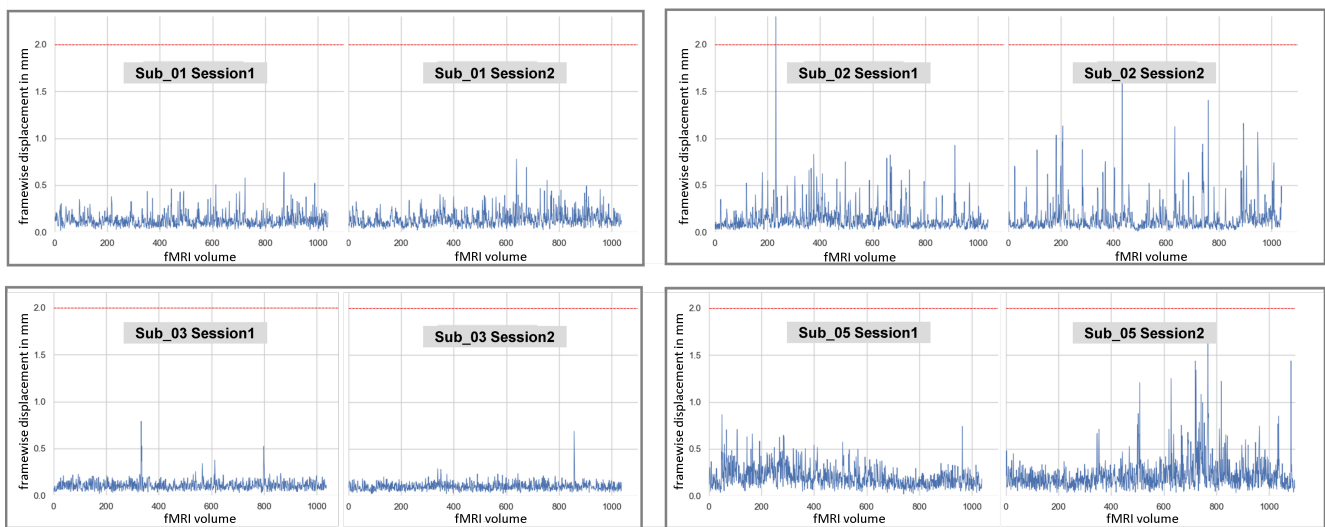


Figure 10. The framewise displacement (FD; in mm) calculated across each subject and session is shown across each volume. The red dashed line indicates the voxel size of the functional images (2x2x2 mm).